Microstructure and hydrogen embrittlement of Q690 bainitic steel welded using electron beam

Pengcong yang

2351627072@qq.com

Ansteel https://orcid.org/0000-0003-3609-7345

Kuijun Fu

Ansteel

Yumin Wu

Ansteel

Jiaji Wang

Ansteel

Fengya Hu

Ansteel

Yulai Song

Jilin University

Research Article

Keywords: hydrogen embrittlement, weld, bainite steel, offshore steel, HIC, cold crack

Posted Date: August 31st, 2023

DOI: https://doi.org/10.21203/rs.3.rs-2930542/v1

Version of Record: A version of this preprint was published at Welding in the World on April 23rd, 2024.
See the published version at https://doi.org/10.1007/s40194-024-01770-0.

Abstract

In this study, Q690 bainitic steel was welded through vacuum electron beam welding under currents of 350 and 500 mA, resulting in samples with different microstructures and fusion and heat-affected zones. Furthermore, H_2S immersion tests were performed to determine the susceptibility of the welded microstructure to hydrogen embrittlement. The results indicated fracture occurrence in the coarse-grain heat-affected zone (CGHAZ) and the fusion zone of the samples welded under currents of 350 and 500 mA, respectively. Under the 350-mA welding current, fracture occurred in the CGHAZ because of the high dislocation density in the bainitic ferrite plates and the low amount of retained austenite in the CGHAZ. Under the 500-mA current, hydrogen embrittlement and fracture occurred because of the high welding-induced heat input that led to coarse precipitation and micro-void coalescence in the upper bainite of the fusion zone.

1 Introduction

Hydrogen embrittlement is a widely observed phenomenon and causes the premature failure of various service weldments. Not only welding introduces hydrogen to the resulting fusion zone, but also service environments such as ocean and underground pipelines environment also introduce hydrogen to the weldments [1, 2]. Additionally, atomic hydrogen can transport within microstructures and diffuse to hydrogen-sensitive stress concentration areas, resulting in fractures induced by hydrogen embrittlement. Thus far, considerable research efforts have been dedicated to investigating hydrogen embrittlement [3–5].

The effects of microstructure on hydrogen embrittlement have been comprehensively investigated. For example, research revealed that austenite exhibits minimum susceptibility to hydrogen embrittlement because its fcc crystal microstructure hinders hydrogen diffusion [6]. By contrast, martensite exhibits maximum susceptibility to hydrogen embrittlement, followed by bainite [7]. Nevertheless, the obtained heat-affected zone microstructures are typically heterogeneous and comprise martensite/austenite and lower bainite [8, 9]. Moreover, fusion zone microstructures may be constituted by both lower bainite and upper bainite[10]. The size of carbides and dislocation density may also influence hydrogen embrittlement. Therefore, the influence of heterogeneous microstructures on the susceptibility to hydrogen embrittlement should be further analysed.

In the present study, Q690 bainitic steels were welded using a vacuum electron beam with different welding currents. Additionally, the fracture mechanisms were investigated, and the results indicated slight changes in the mixed microstructures comprising different weldments, leading to changes in the fracture sites induced by hydrogen embrittlement.

2 Experiment procedure

Q690 bainitic steel plates with dimensions 500 mm × 300 mm × 50 mm were ground. Table 1 lists their chemical compositions. As illustrated in Fig. 1, the Q690 substrates were dominated by lower bainite. An

SEBM80-40A vacuum electron beam welder was used to weld 50-mm thick billets under welding currents of 350 and 500 mA. The voltage and welding speed were maintained at 60 kV and 300 mm/min, respectively. The focus of the electron beam was set below the workpiece surface.

Table 1
Chemical compositions of the steels used in this study (mass fraction)

C	Mn	Cr	Cu	Si	Mo	Ni	P	S	V	Ti	B	Fe
0.08	1.25	0.49	0.26	0.10	0.40	0.85	0.004	0.001	0.04	0.008	0.001	Bal.

The samples were characterized through scanning electron microscopy (SEM, QUAN 400-HV) after immersion in a 4% nitric acid alcohol solution. Subsequently, the microhardness of the samples was measured using a Vickers microhardness tester(FV-300) with a 500 g load. In particular, the coarse-grain area of the welding heat-affected zone was cut into slices and beaten to slices with a thickness smaller than 40 μm, followed by double spraying to reduce the thickness. The microstructures of the CGHAZ corresponding to the different welding currents were characterized through transmission electron microscopy (TEM, Tecnai G2 20).

Standard circular tensile tests were performed on base metal and welded circular tensile parts corresponding to different welding currents. A base-metal circular tensile part and the 350-mA and 500-mA welded circular tensile parts were immersed in a H_2S solution containing 5% NaCl + 0.5% acetic acid for 96 h. After immersion, the post-immersion circular tensile parts were subjected to tensile tests, the experimental procedure as illustrated in Fig. 2. The fracture sections of all the samples were investigated using SEM (QUAN 400-HV). Additionally, the fracture sections were cut in the middle and analysed. The microstructures of fracture sites were investigated using SEM.

3 Results and discussion

3.1 Results of tensile test

Table 2
Results of tensile test

Group	$R_p0.2$ (MPa)	R_m (MPa)	A%	Z%	fracture mode	fracture site
Base metal	763	809	20.52	77	Plastic	Base metal
350-mA welding	746	799	20.34	76	Plastic	Base metal
500-mA welding	701	790	11.52	58	Plastic	HAZ
Base metal + H_2S	759	799	13.16	57	Plastic	Base metal
350-mA welding + H_2S	644	683	4.48	36	Brittle + plastic	Mainly CGHAZ
500-mA welding + H_2S	684	699	3.20	13	Brittle	Mainly FZ

Table 2 lists the results of tensile tests. The 350-mA weldment was fractured at the base metal and exhibited a tensile strength of 799 MPa; the 500-mA weldment was fractured at the heat-affected zone and exhibited a tensile strength of 790 MPa. Moreover, the tensile strengths of both weldments were negligibly lower than that of the base metal, thereby satisfying the requirements. However, the sensitivities of the base metal and the welded zone to hydrogen embrittlement were considerably different. After immersion in the H_2S solution for 96 h, the tensile strength of the base metal and the 350-mA fusion zone were 799 MPa (10 MPa lower than that before immersion) and 683 MPa (116 MPa lower than that before immersion), respectively. The fracture sites of the 350-mA weldment were primarily distributed in the CGHAZ. The fracture sites of the 500-mA weldment shifted from the heat-affected zone to the fusion zone, and the tensile strength was 699 MPa, which was lower than that before immersion by 91 MPa.

3.2 Welded microstructure and microhardness distribution

Figures 3a and 3b illustrate the fusion zone microstructures formed under welding currents of 350 and 500 mA, respectively. The fusion zone microstructure was dominated by upper bainite. Owing to relatively low carbon content, the precipitated carbides were primarily discrete particles instead of continuous layers [11]. Meanwhile, upper bainite carbides in the fusion zone of the 500-mA weldment were large and coarse, likely because of the reduced hardenability due to the high heat input and resulting elemental evaporation in the fusion zone [12]. The two “C” curves in the time-temperature-transformation (TTT) diagram shifted to the upper left because of the reduced hardenability. Moreover, the 500-mA input reduced the cooling rate, and increased the bainite-start temperature (Bs), thus promoting the initiation and growth of precipitates in bainitic ferrite [13, 14]. Figures 3c and 3d display TEM images of the CGHAZ of samples welded under 350 and 500 mA, respectively; the 350-mA bainite plates exhibited a higher dislocation density, thereby promoting hydrogen embrittlement [15]; By contrast, more retained austenite and less martensite were generated under 500 mA because of the reduced cooling rate. The retained austenite content was negatively related to the hydrogen embrittlement susceptibility [7, 16].

Figure 4 illustrates the hardness distribution of samples welded under different welding currents. The hardness of the heat-affected zone of the 350-mA weldment was considerably higher than that of the 500-mA weldment, likely because of the high martensite content in the 350-mA weldment due to the high cooling rate and the high dislocation density of bainite. A 500-mA high heat input welding increased the evaporation of various elements, especially carbon, resulting in drastically reduced hardness. Furthermore, the coarsening of carbides in the fusion zone may reduce hardness. Therefore, the hardness of the fusion zone of the 500-mA weldment was notably lower than that of the 350-mA weldment.

3.3 Fracture sites of welding circular tensile parts induced by hydrogen embrittlement

Figure 5a displays a macroscopic image of the tensile fracture section of the 350-mA welding circular tensile parts after immersion in the H_2S solution for 96 h. The fracture sites were located on the left side of the fusion boundary; the fracture initiated in the CGHAZ and propagated toward the base metal. Figure 5b illustrates the morphology of the welding heat-affected zone of the lower bainite microstructure at the fracture site. Figure 5c illustrates the onset of a hydrogen-induced crack in the unmixed zone or the CGHAZ. Figure 5d displays a macroscopic image of the tensile fracture section of the 500-mA welding circular tensile parts after immersion in the H_2S solution for 96 h. Fracture sites were concentrated in the fusion zone, and some fractures propagated to the welding heat-affected zone.

3.4 Fractography of welding circular tensile parts after immersion in H_2S solution

Figure 6a displays the SEM tensile fractographic images of the macro-morphology of the 350-mA welding circular tensile parts after immersion in the H_2S solution for 96 h. As a zoom-in image of Area b in Fig. 6a, Fig. 6b illustrates hydrogen embrittlement fracture characteristics with quasi-cleavage [17] and slight intergranular fracture characteristics; the image indicates that the length of the brittle fracture was approximately 5.344 mm. Figure 6c depicts plastic fractures with dimple characteristics. Figure 6d displays the SEM tensile fractographic images of the macro-morphology of 500-mA welding circular tensile parts after immersion in the H_2S solution for 96 h. The quasi-cleavage and micro-void coalescence fractures were staggered in the tensile fracture section. The flat region was aligned with the cleavage plane and underwent cleavage fracture; the slope region contained micro-void coalescence fractures. Figure 6e illustrates the quasi-cleavage fracturing mode. Figure 6f displays the fracture morphologies of micro-void coalescence and quasi-cleavage in the upper and lower parts, respectively. According to the Beachem model, micro-void coalescence was the hydrogen-induced fracturing mode with a maximum stress intensity factor and a low hydrogen concentration [18]. Because these micro-voids were generated in the precipitated particle phase of the microstructures [7, 19], the coarsening of the carbides in the upper bainite of the fusion zone may have promoted the generation of such micro-void coalescence fractures and deteriorated the sample performance.

4 Conclusions

Before immersion in the H_2S solution, the tensile strengths of the 350-mA and 500-mA weldments were 799 and 790 MPa, respectively, and fracture occurred in the base metal and heat affected zone, respectively. After immersion in the H_2S solution, the corresponding tensile strengths were 683 and 690.MPa, respectively, and the fracture shifted to the CGHAZ and the fusion zone, respectively.

In the 350-mA weldment, the dislocation density in the lower bainite and content of martensite in the CGHAZ were higher and the content of retained austenite was lower than in the 500-mA weldment. Consequently, after immersion in the H_2S solution of the 350-mA welding circular tensile parts, fracture primarily occurred in the CGHAZ. Thus, the hardenability of the plates of the 350-mA weldment should be reduced.

In the 500-mA weldment, the carbide precipitated in the upper bainite was coarse, thereby promoting hydrogen embrittlement due to micro-void coalescence. Therefore, after immersion in the H_2S solution, fracture occurred in the fusion zone of the 500-mA weldment. Thus, the hardenability of the plates of the 500-mA weldment should be improved.

Declarations

Acknowledgments

We thank the 14th five-year plan of the Ministry of Science and Technology (grant no.2022YFB4601801) for their financial support.

Declaration of interest statement

The authors declare no conflict of interest.

References

1. Satish KS, Sachin M(2017)A review on welding of high strength oil and gas pipeline steels. J Nat Gas Sci Eng 38:203-217.
2. Yue X, Lippold JC(2013)Evaluation of heat-affected zone hydrogen-induced cracking in navy steels. Weld J 92(1):20-28.
3. Song EJ, Suh DW, Bhadeshia HKDH(2013)Theory for hydrogen desorption in ferritic steel. Comput Mater Sci 79:36-44.
4. Michler T, Naumann J(2010)Microstructural aspects upon hydrogen embrittlement of various bcc steels. Int J Hydrogen Energy 35:821-832.
5. Song EJ, Bhadeshia HKDH, Suh DW(2013)Effect of hydrogen on the surface energy of ferrite and austenite. Corros Sci 77:379-384.

6. Sunilkumar D, Shaikh H, Dey HC, Albert SK(2021)Remedies for hydrogen-embrittlement on Grade-91 steel weld joint during long delay in PWHT. Weld World 65:833-844.
7. Lippold JC(2015)Welding metallurgy and weldability. Hoboken (NJ): John Wiley and Sons; 2015.
8. Di XJ, Tong M, Li CN, Zhao C, Wang DP(2019)Microstructural evolution and its influence on toughness in simulated inter-critical heat affected zone of large thickness bainitic steel. Mater Sci Eng A 743:67-76.
9. Yang XC, Di XJ, Liu XG, Wang DP,Li CN(2019)Effects of heat input on microstructure and fracture toughness of simulated coarse-grained heat affected zone for HSLA steels. Mater Charact. 155:109818.
10. Zhang T, Li Z, Ma S, Kou S, Jing H(2016) High strength steel (600–900MPa) deposited metals: microstructure and mechanical properties. Sci Technol Weld Joi 21:1-8.
11. Bhadeshia HKDH, Honeycombe RWK(2017)Steels: microstructure and properties. 4nd end. London: IOM Communications.
12. Block-Bolten A, Eagar TW(1985) Metal vaporization from weld pools. Metall Mater Trans B 15(3):461-469.
13. David AP, Kenneth EE, Mohamed YS(2009)Phase Transformations in metals and alloys. 3rd ed. Boca Raton (FL): Talor & Francis, CRC Press.
14. Hozweissig MJ, Canadinc D, Maier HJ(2012)In-situ characterization of transformation plasticity during an isothermal austenite-to-bainite phase transformation. Mater Charact 65:100-108.
15. Robertson IM, Sofronis P, Nagao, Nagao A, Martin ML, Wang S, Gross DW, Nygren KE(2015)Hydrogen embrittlement understood. Metall Mater Trans B 46:1085-1103.
16. Bhadeshia HKDH(2016) Prevention of hydrogen embrittlement in steels. ISIJ Int 56:24-36.
17. Martin ML, Fenske JA, Grace SL, Sofronis P, Robertson IM(2011) On the formation and nature of quasi-cleavage fracture surfaces in hydrogen embrittled steels. Acta Mater 59:1601-1606.
18. Beachem CD(1972) A new model for hydrogen-assisted cracking (hydrogen “embrittlement”). Metall Mater Trans B 3:441-455.
19. Chen Y, Lu H, Liang J, Rosenthal A, Liu H, Sneddon G, Mccarroll I, Zhao Z, Li W, Guo A, Cairney JM(2020)Observation of hydrogen trapping at dislocations, grain boundaries and precipitates. Science 367:171-175.

Figures

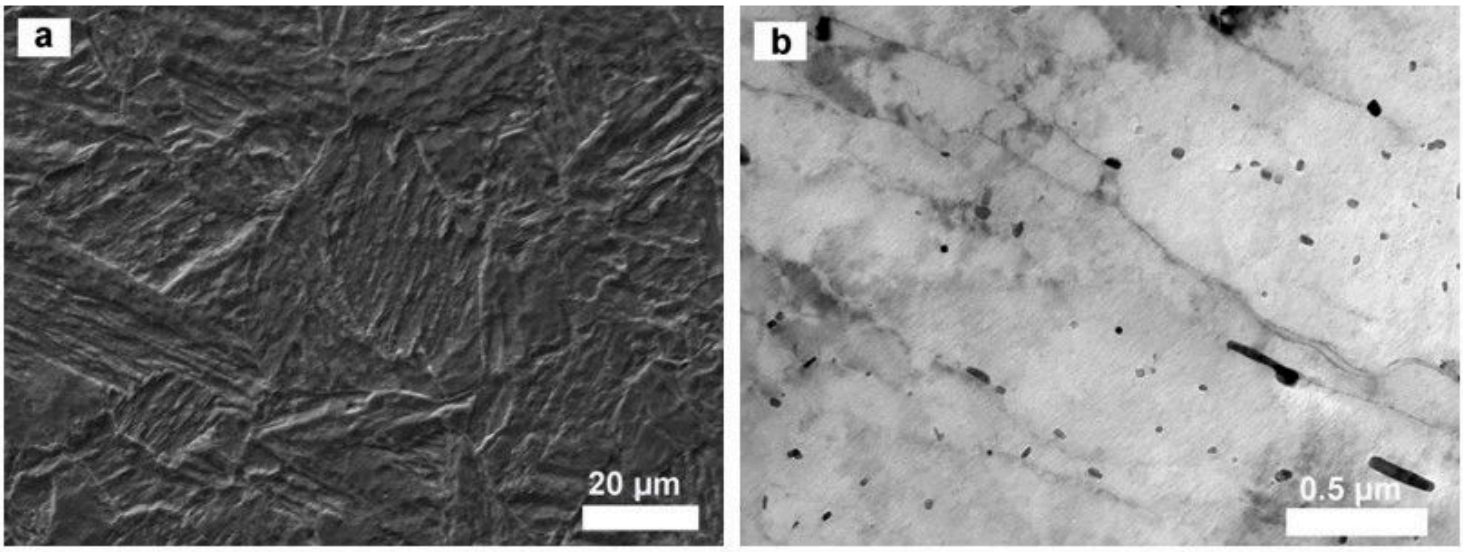

Figure 1

Characterization of matrix microstructure through (a) SEM and (b) TEM

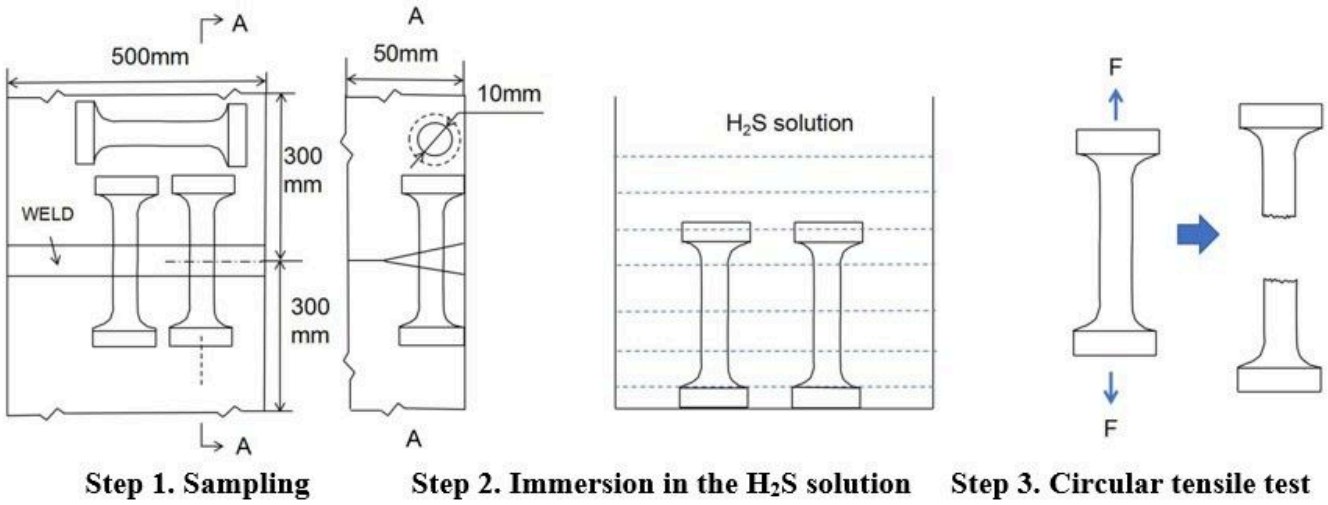

Figure 2

Schematic of the experimental procedure

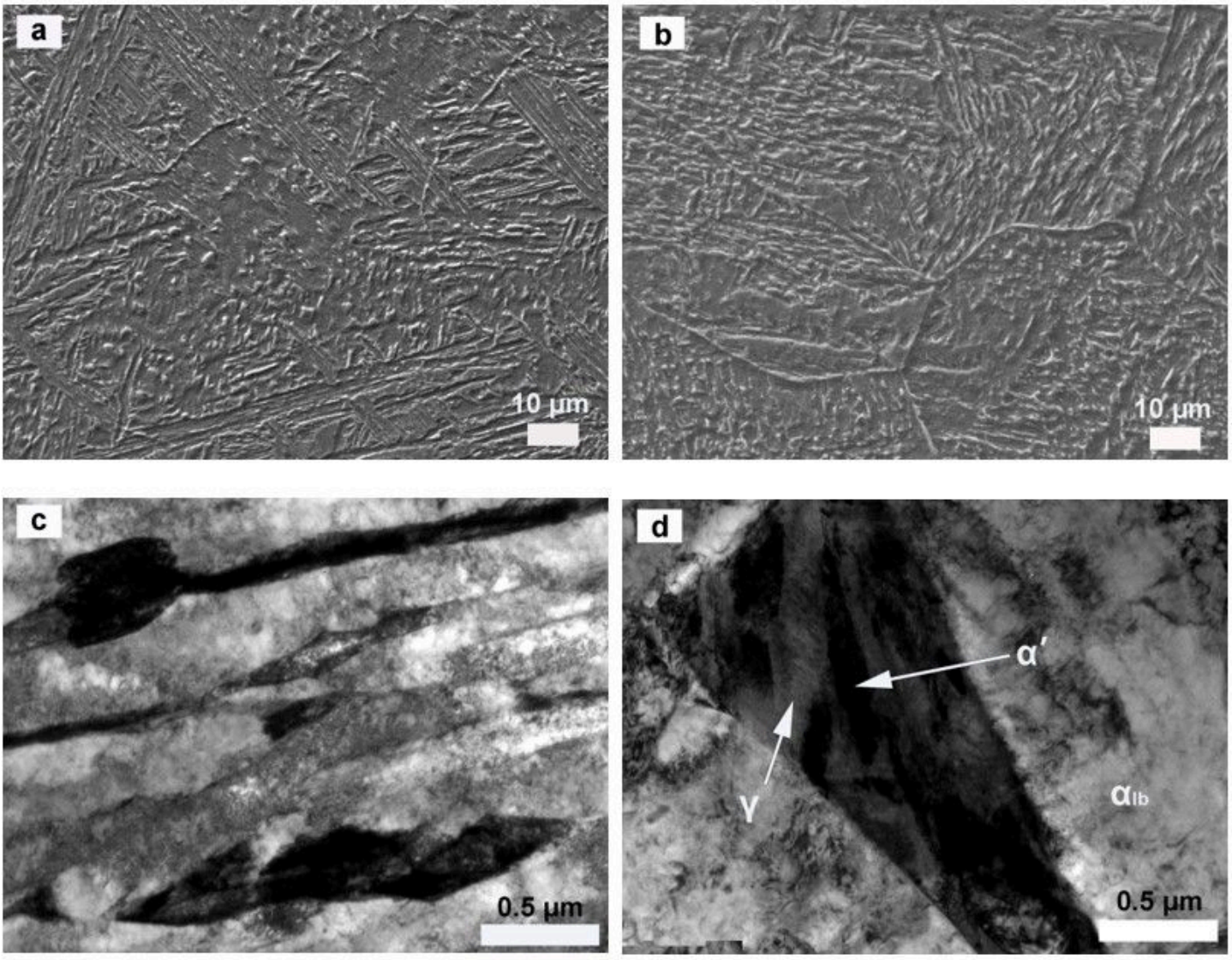

Figure 3

Microstructures of the fusion zone and coarse-grain heat-affected zone (CGHAZ) under different welding currents: (a) SEM image of the fusion zone under a welding current of 350 mA; (b) SEM image of the fusion zone under a welding current of 500 mA; (c) TEM image of the CGHAZ under a welding current of 350 mA; (d) TEM image of the CGHAZ under a welding current of 500 mA (α' represents martensite, γ represents retained austenite, and α_{lb} represents lower bainite).

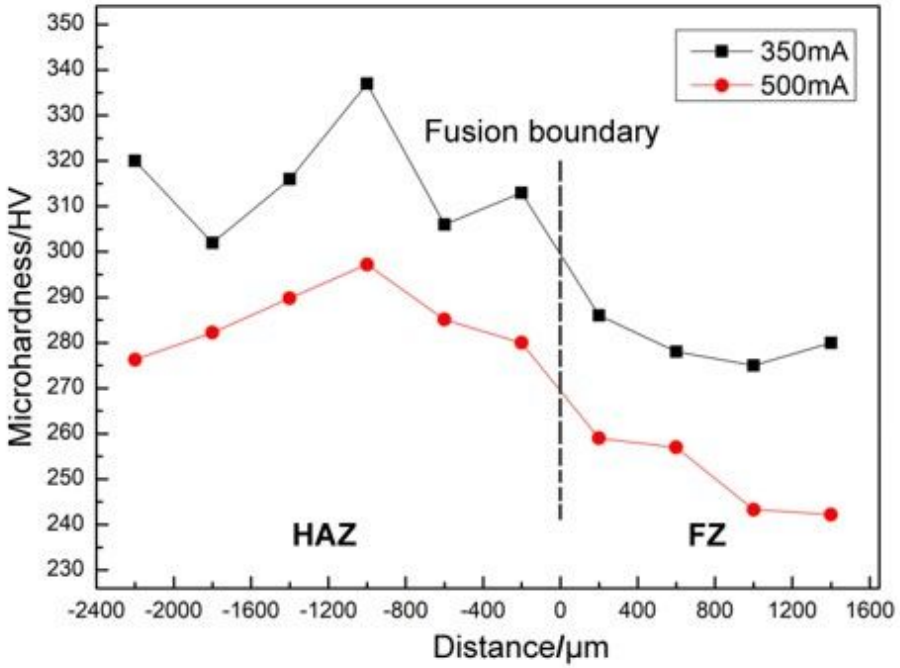

Figure 4

Distribution of the micro-hardness of samples welded under different welding currents (HAZ represents heat affected zone, FZ represents fusion zone).

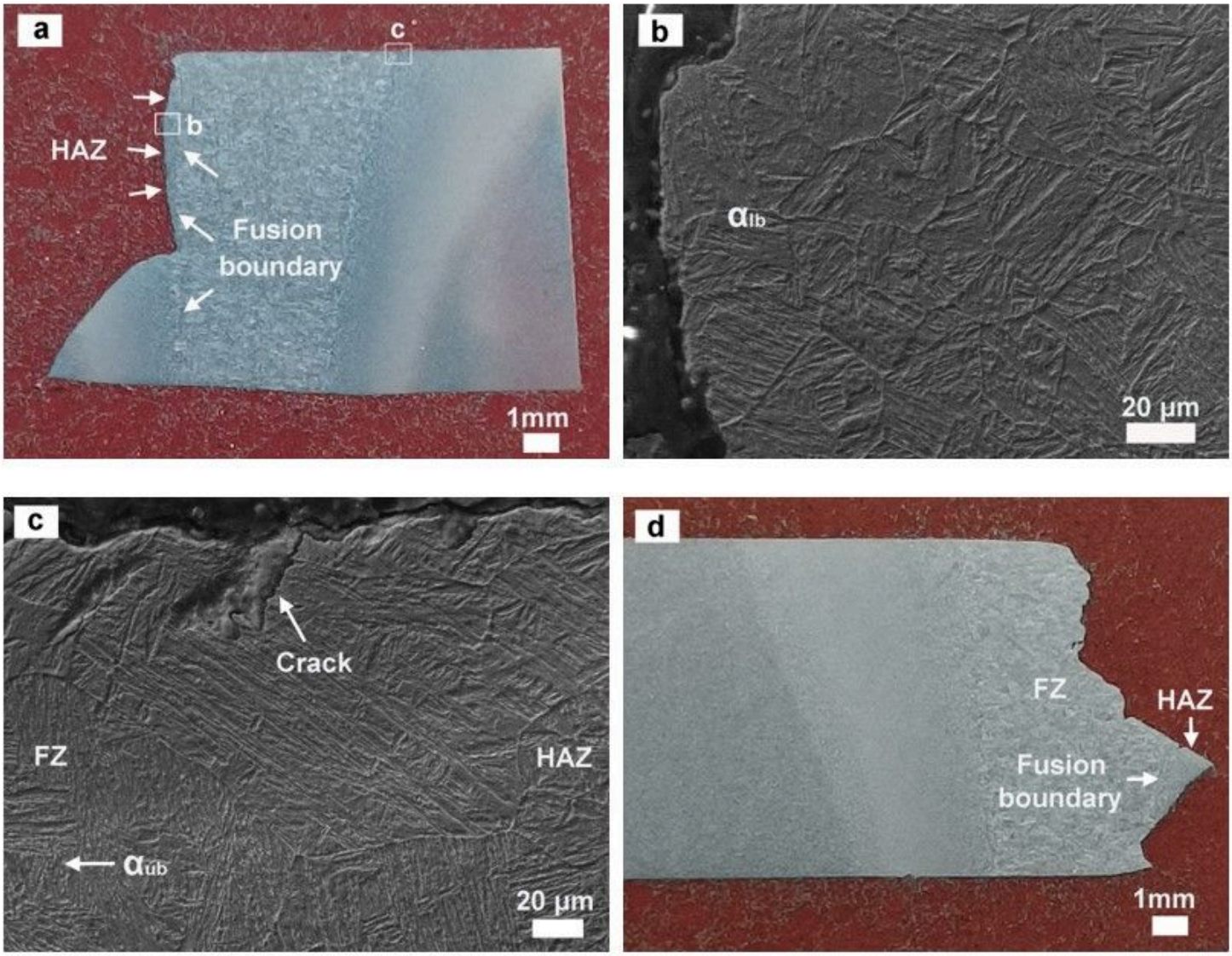

Figure 5

SEM fractographic images of the circular tensile parts after immersion in the H_2S solution for 96 h under different welding currents: (a) 350 mA; (b) and (c) zoom-in view of (a). (d) 500 mA (α_{ub} denotes upper bainite).

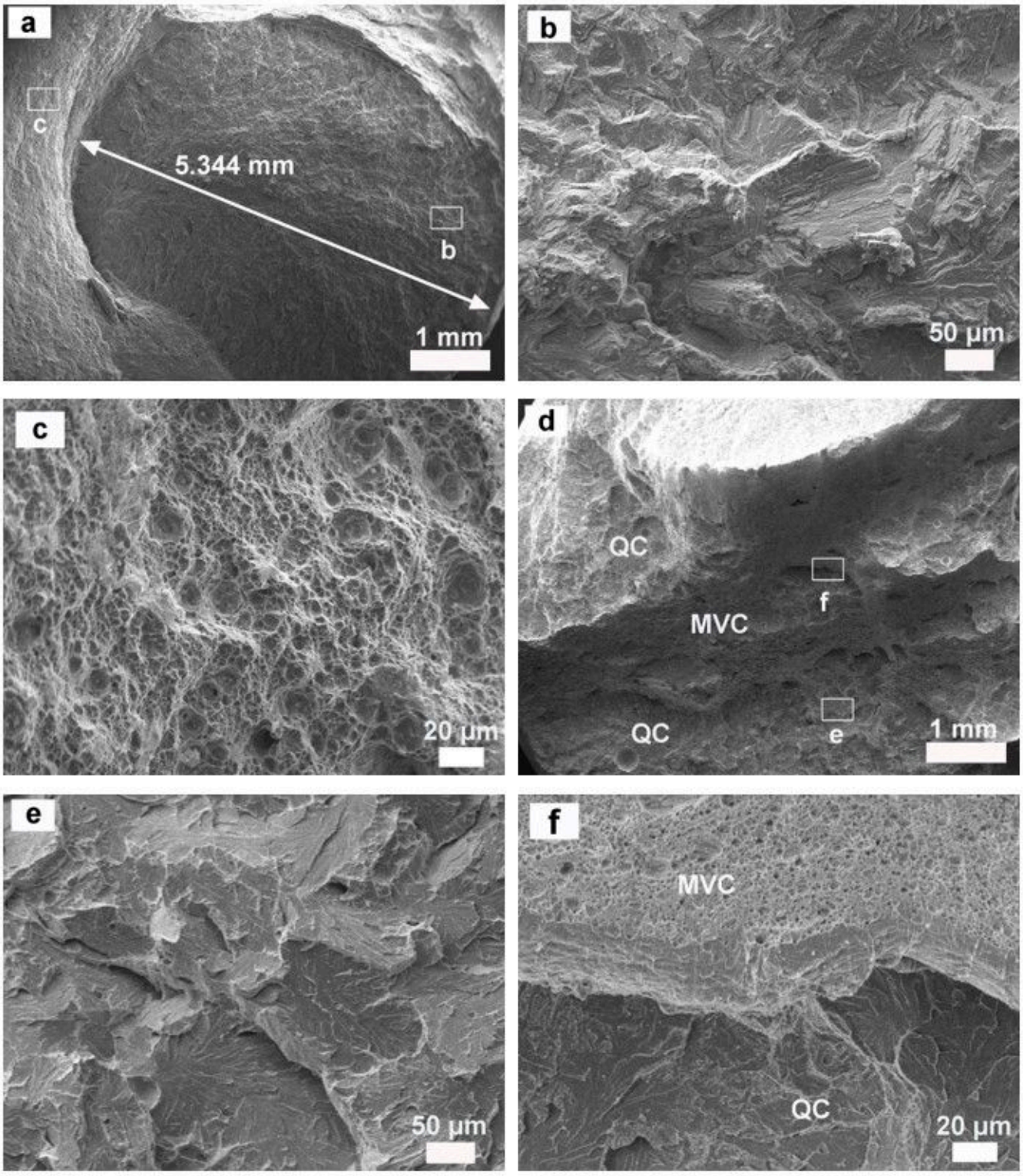

Figure 6

SEM fractographic images of the circular tensile parts under different welding currents after immersion in the H_2S solution for 96 h: (a) 350 mA; (b) and (c) are the zoom-in images of (a); (d) 500 mA; (e) and (f) are the zoom-in images of (d); (MVC denotes micro-void coalescence, QC denotes quasi-cleavage).